Electrowetting dynamics of sessile droplets in a viscous medium

Juan S. Marin Quintero ⬤, Butunath Majhy ⬤, and Prashant R. Waghmare ⬤[*]
Interfacial Science and Surface Engineering Lab (iSSELab), Department of Mechanical Engineering,
University of Alberta, Edmonton, Alberta, Canada T6G2G8

Electrowetting is a technique that reversibly or irreversibly alters the wetting properties of a droplet on a hydrophobic substrate by applying an electrical field. In this paper, we studied electrowetting dynamics of sessile droplets on a hydrophobic substrate surrounded by viscous liquids. Through this study, we answered the following unanswered questions: the drop's transient response immediately after the actuation, the drop's retraction and resultant dynamics, and the effect of multiple wave actuation on the droplet transition. An overall energy balance approach is extended for analyzing the transient wetting dynamics of droplets from the initial position to the new equilibrium position in viscous media with appropriate governing parameters. The governing nondimensional parameters are the electrowetting number (η), the Roshko number (Ro), the Ohnesorge number (Oh), and the viscosity ratio (μ_r) between the droplet and the surrounding medium. This theoretical study, in corroboration with the experimental study, describes the transient evolution of the drop motion from the initial position to the new equilibrium position and predicts the shift from in-phase to out-of-phase drop response for the applied waves.

I. INTRODUCTION

Electrowetting is the induced spreading of an electrolyte aqueous liquid droplet on a hydrophobic surface by applying an electrical potential [1]. It has a wide range of applications such as microfluidic mixing [2–4], liquid lenses [5,6], droplet transport [7,8], and clinical diagnostics on human physiological fluids [9]. In 1875, this phenomenon was discovered by Lippmann [10], who observed that by applying a voltage difference between an aqueous solution and mercury, the liquid-liquid interface on a capillary could be controlled. In the case of electrowetting, an electrical double layer is spontaneously formed at the solid-liquid interface upon voltage application, which is made up of ions and counterions. The magnitude of the applied potential difference is tuned to control the charge distribution that reflects the slip at the contact line [11]. Thus, electrowetting is commonly characterized by quantifying the change in equilibrium contact angle (θ). The new equilibrium contact angle (θ), due to the applied voltage, can be deduced by energy minimization, commonly known as the Young-Lippmann (Y-L) equation [1], $\cos\theta = \cos\theta_0 + \frac{\epsilon_0 \epsilon_d U^2}{2d\sigma} = \cos\theta_0 + \eta$. The Y-L equation predicts the change of the contact angle for the applied voltage at the equilibrium. However, it fails to comment on the dynamic evolution and transience involved in the droplet configuration before equilibrium, particularly for ac scenarios. Thus, the drop's transience response immediately after the voltage is unknown, meaning the droplet dynamics are unknown during the initial time period. A few studies [12–20] have focused on the role of applied frequency and its implication on the equilibrium contact angle, but the transience involved in this process is always missing. Hence, it is not fully understood how the drop attains the steady state and how the system parameters

---

*waghmare@ualberta.ca

024001-1

play a role in it. Therefore, we proposed an energy conservation approach rather than a simplistic scaling analysis that fails to comment on transient variations of different energy terms associated with this phenomenon. Here, the drop's transient response is analyzed for electrowetting parameters, applied frequency, and the medium viscosity by governing appropriate nondimensional parameters like the electrowetting number (η), the Roshko number (Ro), the Ohnesorge numbers (Oh), and the viscosity ratio (μ_r). Finally, the dynamic response of a drop for a sequence of electrowetting waves was studied in detail.

The dynamic response of the liquid lenses by electrowetting is similar to the present sessile droplet actuation dynamics [21]. Understanding the temporal dynamics of electrowetting-on-dielectric (EWOD) devices, especially the response time, is important for many applications [21,22]. Recently, microscopes incorporating EWOD lenses have been demonstrated, enabling nonmechanical depth scanning [22]. EWOD prisms have also been used for nonmechanical beam steering and show promise for light detection and ranging and remote sensing applications. However, achieving fast response times from these devices is one of the main challenges. For instance, a typical confocal microscope uses a pair of galvanometer mirrors for two-dimensional lateral scans at kHz frequencies. Using a liquid lens in such a microscope would allow for a large depth scan; however, the response time of such an element needs to be comparable to the lateral scanning speed. The complete understanding of the drop's response can increase the efficiency of EWOD-based devices by reducing operation times and having the entire description of the drop's evolution for a given actuation. It is desirable to generate relatively simple models that can describe and predict the transient evolution of the drop spreading [23–25]. Thus, the objective of the present paper is to investigate and develop a theoretical approach that considers the effect of electrowetting and the fluids' properties, which can give a better understanding starting from the drop's initial response to the transient dynamics until the new equilibrium position. The overall energy balance (OEB) approach is extended to study the sessile drop configuration in a varied viscous medium, unlike the force balance concept in the Y-L equation. This model describes the transient evolution of the drop motion, and predicts the shift from in-phase to out-of-phase drop response from the applied waves.

The experiments were conducted by depositing 3-μL drops of aqueous solution [deionized (DI) water and 0.1M sodium chloride] in viscous oil media. A disposable syringe was used to generate the drops inside a distortion-free cuvette, which was prefilled with silicone oil (Paragon Scientific, Ltd.) with different viscosities (see Table I in the Supplemental Material [26]). The drops were deposited on a copper substrate, which was coated with a thin layer (20 μm) of polydimethylsiloxane (PDMS), acting as electrode and dielectric ($\varepsilon_d = 2.8$), respectively. The actuation by means of electrical signal was triggered by a waveform generator (294 100MS/s, FLUKE), which was further augmented by an amplifier (BOP 500, KEPCO) to obtained the desired output. Finally, a copper wire, with a diameter of 60 μm, was used as positive electrode, and it was situated at the center of the droplet but with a separation distance equal to the initial radius of the drop from the bottom electrode. The drop's perturbation and the associated changes in the shape of the drop were recorded with a high-speed camera (Phantom V711, Vision Research Inc.) with a frame rate of 3000 frames per second. The captured videos were calibrated and postprocessed with an image analysis software (ImagePro Premier 9.2, Media Cybernetics, Inc.) for the quantification of instantaneous drop height and contact angle. The drops attained an equilibrium, or initial height of $h_0 = 1.70 \pm 0.03$ mm with an associated contact angle $\theta_0 = 154 \pm 5.7°$ in different mediums. However, the initial height and initial contact angle for the numerical study were selected as $h_0 = 1.70$ mm and $\theta_0 = 153.5°$, respectively.

II. MATHEMATICAL MODEL

Here, the sessile drop is sufficiently small, and the gravity has negligible effect compared to the capillarity. Therefore, it is safe to assume that the sessile drop shape resembles a spherical cap as shown in Fig. 1(b). By simple geometric exercise, the volume of the spherical cap can be deduced as presented in Eq. (1), which is a function of the radius of the sphere, r, or the height of the sessile
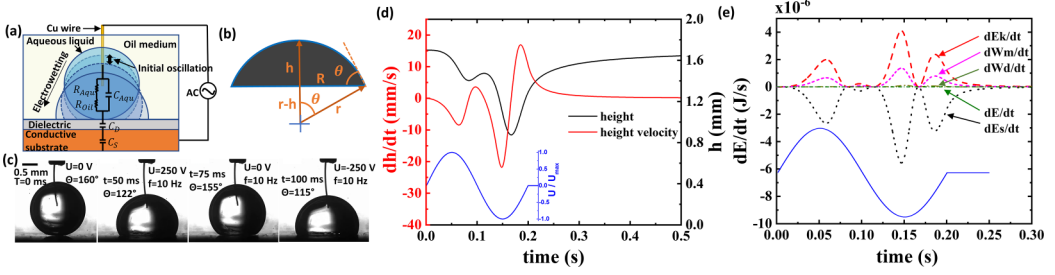
FIG. 1. (a), (b) Schematic illustrations of (a) electrowetting of the aqueous droplet in a liquid medium when it is subjected to the ac electric field and (b) truncated spheroid shape of the droplet. (c) Initial transient response (immediately after the voltage is applied) of the aqueous droplet of ($V = 3\,\mu$L, $\mu_d = 0.91$ mPa s) in a silicone oil ($\mu_m = 100.60$ mPa s) medium subjected to a sine wave of $U_{ac} = 350$ V at a frequency $f = 10$ Hz from experiment. Theoretical results for the corresponding droplet are illustrated as (d) height and the rate of change of height with respect to time and (e) comparison of all the different energies considered in the theoretical model.

drop, h, and the contact angle, θ, as

$$V = \frac{\pi h^3}{3} \frac{2 + \cos\theta}{1 - \cos\theta}. \tag{1}$$

For a constant drop volume, after ignoring the evaporation, the relationship between the transient variation in the contact angle and the height can be established as follows:

$$\frac{d\theta}{dt} = \left(\frac{(2 + \cos\theta)(1 - \cos\theta)}{h\sin\theta} \right) \frac{dh}{dt}. \tag{2}$$

For a higher voltage of actuation ($\geqslant 350$ V) in liquid media, the shape of the droplet changes from a truncated spheroid to a truncated oblate shape. Then, we have to consider the truncated oblate shape and corresponding correlation, which is discussed in detail in Sec. I in the Supplemental Material [26].

To theoretically determine the implication of induced drop deformation, due to applied electric actuation by means of electrowetting, the OEB approach is considered. The variation of the drop's height can be predicted with different energies involved in this process, namely, kinetic, surface, and viscous dissipation due to drop and surrounding medium. Considering the sessile drop as the control volume, the applied electric energy (E_{in}) is utilized to move the contact line, i.e., the creation or destruction of the interfaces at a certain velocity (U_d). For this system, the energy balance can be written as

$$\frac{dE_{in}}{dt} = \frac{d}{dt}(E_k + E_s) + \frac{d}{dt}(W_d + W_m). \tag{3}$$

Here, E_{in} is the energy added to the system, and E_k and E_s are the kinetic and the surface energies of the drop. An additional work must be done to overcome the inherent resistance caused by the viscosity of the drop (W_d) and medium viscosity (W_m). In the Supplemental Material [26], the expressions for all necessary energies that govern the energy balance are studied individually. The variation in the drop's height due to oscillatory actuation of the drop in another liquid medium is

$$\frac{m}{(2 + \cos\theta)^2} \frac{d^2h}{dt^2} + \frac{m(1 - \cos\theta)}{h(2 + \cos\theta)^2} \left(\frac{dh}{dt} \right)^2 + \left(\frac{8\pi(\mu_d + \mu_m)h}{\sin^3\theta} \right) \left(\frac{dh}{dt} \right)$$

$$+ \frac{2\pi h\sigma}{1 - \cos\theta}[\cos\theta_0 - \cos\theta] = 0. \tag{4}$$

Here, the time dependent instantaneous equilibrium contact angle, θ, is calculated from the modified Y-L equation, $\cos\theta = \cos\theta_0 + \eta \sin^2(2\pi f t)$. Furthermore, the mass of the drop is contemplated as $m = \Delta\rho V$, where V is the volume of the spherical cap, and $\Delta\rho = \rho_d - \rho_m$ is the density difference between drop and medium. To extract the key parameters from the governing equation, the governing equation was nondimensionalized as presented in Eq. (4). It is to be noted that the instantaneous contact angle and drop height are two dependent parameters in this nonlinear second-order ordinary differential equation. With this approach, we have obtained a set of nondimensional numbers for which the characteristic length and timescale were chosen as the drop's initial height (h_0), the inertia-capillary timescale [$\tau_c = (\Delta\rho h_0^3/\sigma)^{1/2}$], and the viscoinertial (momentum) relaxation time ($\tau_m = \Delta\rho h_0^2/\mu$), respectively [36]:

$$\frac{h^{*2}}{3(1 - \cos\theta)(2 + \cos\theta)}\frac{d^2h^*}{dt^{*2}} + \frac{h^*}{3(2 + \cos\theta)}\left(\frac{dh^*}{dt^*}\right)^2$$

$$+ \text{Oh}\left(\frac{8}{\sin^3\theta}(1 + \mu_r)\right)\left(\frac{dh^*}{dt^*}\right) + \frac{2(\cos\theta_0 - \cos\theta)}{1 - \cos\theta} = 0. \tag{5}$$

Here μ_r is the ratio of the medium to the drop's viscosity, and Ohnesorge number $\text{Oh} = \mu_d/(\Delta\rho\sigma h_0)^{1/2} = \tau_c/\tau_m$ is the ratio between these two timescales (and t is in units of τ_c). Writing time in units of τ_c leads to $ft = \frac{f}{1/\tau_c}\frac{t}{\tau_c} = f^*t^*$ with the frequency measured in units of the capillary frequency of the oscillator. For frequency in units of the momentum relaxation τ_m, we write $\frac{f^*}{\tau_m}t^* = \frac{f}{\tau_m}\frac{\tau_m}{\tau_c}t^* = \text{Ro Oh}t^*$. In this nondimensionalization process, the equilibrium contact angle gets appropriately changed to $\cos\theta = \cos\theta_0 + \eta\sin^2(2\pi\text{Ro Oh}t^*)$, where $\text{Ro} = fh_0^2\Delta\rho/\mu_d$ is the Roshko number. In the present analysis, the solution of this second-order differential equation was obtained with a fourth-order Runge-Kutta method with $h^* = 1$ and $dh^*/dt^* \approx 0$ as initial conditions. The proposed theoretical model is validated with the experimental results for a range of μ_r (10–1000), η (0.29–0.89), and Ro (0.44–44.49). Table II in the Supplemental Material [26] rendered different experimental data sets where the same value of the nondimensional parameters is achieved by various combinations of physical variables with constant drop volume ($d = 2$ mm, $h_0 = 1.6$ mm) and drop viscosity ($\mu_d = 0.91$ mPa s). The variation in the Oh for the considered parameters is marginal from $\approx 8.9\times10^{-3}$ to 9.7×10^{-3}, hence we have not considered this in our parametric analysis. In the upcoming section, experimental details are reviewed before the discussion of the comparison between the theoretical model and the experimental evidence.

III. RESULTS AND DISCUSSIONS

Interestingly, when an aqueous droplet (DI water and $0.1M$ sodium chloride of 3-μL volume surrounded by a silicone oil medium on a copper substrate embedded with a dielectric PDMS layer) is subjected to an ac electric field (250 V, $f = 10$ Hz) [see Fig. 1(a) for schematic illustrations], the aqueous droplet reversibly wets and dewets the surface (see video 1). The electrical analogy shown in Fig. 1(a) is discussed in detail in Sec. II in the Supplemental Material [26]. However, if we focus on the initial transient response, the droplet behaves differently (partial spreading) over the dielectric (see video 2). Figure 1(c) shows the initial transient response (immediately after the voltage is applied) of the aqueous droplet in a silicone oil medium subjected to a sine wave of $U_{\text{ac}} = 350$ V at a frequency $f = 10$ Hz from experiment. So, first, we discuss the initial transient response of the aqueous droplet.

For initial transient dynamics, the governing Eq. (5) is solved for the drop's height or the drop-medium interface velocity as shown in Fig. 1(d). Moreover, this equation is a combination of different energy sources that can easily be quantified separately. An analysis of the relative magnitude of the different energies considered with respect to time, as depicted in Fig. 1(e), provides an understating of the drop's oscillations associated with the applied force. Figure 1(d) presents the height and the change in the height of the drop with the time for the case of nondimensional

parameters of Ro $= 0.22$, Oh $= 0.0093$, $\eta = 0.89$, and $\mu_r = 110$. The height's velocity has a zero magnitude at the initial position, and when the voltage turns to a zero value. Also, the velocity asymptotically attains a zero velocity as the drop returns to the initial position. At this point, all the energies return to a zero value as shown in Fig. 1(e). Also, it can be seen that the surface energy is transmitting the energy to the drop in the form of velocity (kinetic energy) and the surroundings as viscous dissipation (work due to drop and medium dissipation). The kinetic energy for almost the entire process was three times bigger than the work due to dissipation, and so the kinetic energy represented approximately 75% of the dielectric energy. It is worthwhile to mention that the negligible work due to the drop's viscous dissipation remained approximately 0.2% of the dielectric energy, which is consistent with the viscosity ratio for this particular case. The maximum energy delivered to the system is nearly at $t = 0.15$ s, which corresponds to the 75% of the period of the wave. At this point, the kinetic energy and the work due to medium dissipation reach their maximum value, while the surface potential energy reaches its minimum. This behavior aligns with the application of the external force perturbation, where there are two moments when the voltage acquires the maximum amplitude, i.e., at 25% ($t = 0.05$ s) and at 75% ($t = 0.15$ s) of the applied period. At these two points, the instantaneous equilibrium contact angle is equal to the apparent contact angle from the Young-Lippman equation, and so the difference between the equilibrium contact angle and the actual contact angle is the highest. However, when the electrical wave is at 25% of its period, the drop is still in an intermediate spreading point where the height velocity is not maximum, the minimum height has not been reached yet, and the substrate-droplet area (A_{SD}) has not reached its maximum value. Therefore, the energies attain their peak when the voltage is maximum for the second time. The asymmetric spreading of the drop between the first half and second half of the electrical wave is detailed in the upcoming sections. Following this order of ideas, a better understanding of the different nondimensional parameters is required to completely understand the drop's response and the oscillations linked with the application of a single or a sequence of electrical sinusoidal waves.

A. Effect of the electrowetting number

The electrowetting number ($\eta = \frac{\epsilon_0 \epsilon_d U^2}{2 d \sigma}$) represents the ratio of the electrostatic energy to the surface energy, and it is the main governing parameter for a sessile droplet perturbed by an electric field. The literature already reported that by increasing the electrowetting number, the apparent contact angle reduces [1], which leads to a lower instantaneous equilibrium contact angle (see Sec. III and the classical electrowetting curve as shown in Fig. S3 in the Supplemental Material [26]) that dictates the solution of Eq. (5). Figure 2(a) illustrates the variation of the nondimensional height of the droplet under ac electrowetting for different values of electrowetting number. The multiplication of the nondimensional time by the Ohnesorge and the Roshko numbers in the x axis facilitates the analysis and comparison of the drop's dynamic response, which translates the time into the number of electrical cycles applied. For fixed values of Oh, Ro, and μ_r, the traditional outcome is observed, i.e., a higher height diminution with the electrowetting number η. The voltage range, and therefore the electrowetting number's range, was selected based on the dielectric breakdown of the insulator layer (the PDMS layer) that is a function of the dielectric thickness depicted as $E_{\text{breakdown}} = 19$ V μm^{-1}. Thus, the maximum possible potential is approximately 400 V before the occurrence of the electrolytic process. Yet, the maximum applied voltage was selected as 350 V ($\eta = 0.89$) to avoid electrolysis and the saturation of the contact angle [37,38]. The lower limit, 200 V ($\eta = 0.29$), was chosen to observe a change in the drop's shape due to electrowetting. The height reduction for waves below this threshold voltage was observed to be less than 5%, inconvenient for capturing the drop's response with the high-speed camera and impractical to compare with the mathematical model. For waves that generate a significant change in the drop's height, it can be seen that the drop does not symmetrically stretch following the applied sine wave. The drop deviates from attaining the forced equilibrium contact angle due to the additional resistance from the surrounding medium, which leads to the dissipation of energy and to the delay
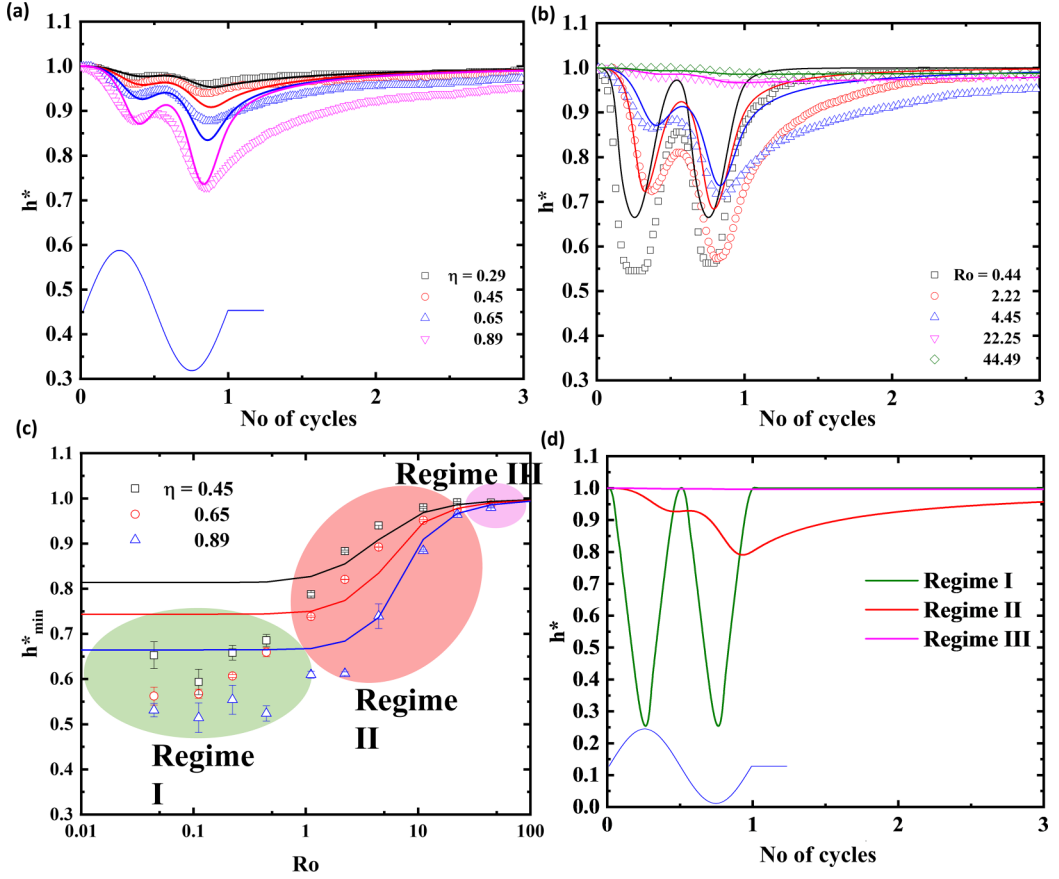
FIG. 2. (a) Transient variation of the droplet height for different electrowetting numbers. The additional terms are fixed to Oh = 0.009, Ro = 4.45, and μ_r = 110.55. (b) Transient variation of the droplet height for different Roshko numbers. The additional terms are fixed to Oh = 0.009, μ_r = 110.55, and η = 0.89. The experimental results are represented by symbols and the results obtained from the proposed model are represented by the solid lines. (c) Effect of Roshko number on drop spreading dynamics. Minimum height achieved by a drop (Oh = 0.009 and μ_r = 110.55) by a single electrowetting wave as a function of Roshko number, for different electrowetting numbers. The experimental results are represented by open symbols, and the lines represent the theoretical results. (d) Three different regimes proposed to study the transient response of drop spreading, which can be categorized into in-phase, out-of-phase, and nonresponsive behavior.

in the spreading. This can be further seen as the drop in the first quarter of the cycle spreads to an intermediate position, which does not correspond to the height calculated from the Young-Lippmann equation. After the first quarter of the cycle, when the voltage is starting to decrease, the drop momentarily continues to spread due to inertia, until it reaches a local minimum. As the voltage significantly reduces in magnitude, and the inertia vanishes in the second quarter of the cycle, the drop recoils to regain its original shape, but at a slower rate compared to the spreading in the first half. This phenomenon is directly attributed to the governing forces acting on the drop; i.e., during the first quarter of the cycle, the electrowetting is forcing the motion, while in the second quarter of the cycle the electrowetting weakens, and the drop follows only the forces imposed by the interfacial tension. Before the drop can arrive at its original height, the second half of the electrical cycle starts, and the voltage restarts, increasing in magnitude, leading to an additional spreading stage of the drop. However, in this second half of the actuation cycle, the drop further spreads due to the partial

spreading occurred in the first half of the cycle. Then, a similar episode occurs as the voltage reaches again its maximum value at $\text{Oh Ro}\,t^* = 0.75$, where it can be seen that the drop retraction is delayed due to inertia. Once the electrical cycle has been completed, the drop monotonically retracts to its original shape regardless of the applied voltage. Nevertheless, it is worthwhile to observe how the drop reattains the initial position in a similar manner after the electrical wave vanishes.

B. Effect of the Roshko number

The nonsymmetric response of the electrowetting is directly related to the relaxation time of the drop and how fast the external force is applied [17]. As a consequence, there is an interplay between the properties of the liquids and the actuation by means of electrowetting. Hence, there are two key aspects one has to compare, the applied actuation frequency and the response in the drop oscillations ($\tau_m = h_0^2 \Delta \rho / \mu_d$), which is mostly due to the viscosity of the droplets. The first natural choice, in the case of considering nondimensional number, can be the Strouhal number St, but we opted for the Roshko number ($\text{Ro} = f h_0^2 \Delta \rho / \mu_d = f / \tau_m$) instead. Roshko [39] introduced this nondimensional group as a dimensionless frequency to study vortex shedding in turbulent flows. Although Ro is commonly used to describe repetitiveness of vortex-street structures, in this paper we propose to use it to represent the repetitiveness in the drop's oscillations. This also allows us to circumvent the use of contact line velocity for the analysis. For this research, Ro describes the oscillating flow mechanisms and directly relates the applied frequency (f) and the drop's viscosity as the governing factors. We consider the viscocapillary timescale ($t^* \sim \mu d / \sigma$), which considers viscous and surface tension force, but fails to account for the actuation frequency. With the definition of t^* for considered parameters, it is 0.02 ms, whereas our observation timescale is from 0.1 to 500 ms. The applied frequency is from 1 to 100 Hz; hence actuation frequency timescale is an appropriate representation of the characteristic timescale. Thus, we have considered the Roshko number for our analysis, which is applied frequency in units of the momentum relaxation time (τ_c).

Figure 2(b) represents the response of the drop's height to the varied range of the Ro number, where Ro is varied from 0.44 to 44.49. In any damped harmonic oscillator system, the existence of the resonance frequency can significantly alter the oscillations. The first resonance frequency for a drop of 3 µL in an oil medium is approximately $f_2 \approx 35$–40 Hz [40]. Therefore, we avoided frequencies close to this, to avoid any implication from the resonance. Based on the experimental observations it was noticed that beyond 100 Hz the drop's response was minimal; therefore, the highest frequency selected was 100 Hz (Ro = 44.49). With this frequency a noticeable response in the drop's shape was observed. Below a certain frequency, the drop has a tendency to slip away from its center, also reported as "waggling" [18]. Therefore, to avoid any asymmetric linear translation in the drop along the spreading direction, the lowest frequency of 1 Hz (Ro = 0.44) was chosen. For this lowest frequency, i.e., for Ro = 0.44, it is clearly seen that the drop closely follows a symmetric spreading and both valleys, representing the minimum height in the drop, have a similar magnitude. The symmetric or uniform spreading of the drops is defined to be fulfilled if the difference between the magnitude of droplet's height at the maximum spreading position in both halves has a difference below 5%. The discrepancy between the experimental and theoretical predictions is off twofold: first, the predicted magnitude in the drop's height, and second, the location of the minima. Interestingly, the time achieved to attain minima matches quite well with the experimental observations. The underprediction of height depression is significant for lower Ro, but for higher Ro (4.45 and above) it matches well. The proposed model is developed for ac voltage, whereas the lower frequency behaves similarly to dc voltage scenario; hence, the discrepancies can be justified.

For a relatively low frequency (Ro = 0.44), the drop's response is in phase with the actuation, as we observed in the case of η. As Ro is increased, the actuation timescale is much faster than the response of the drop. Hence, the deviation from the actuation cycle is observed in the case of Ro = 2.22 and above. As a result, the drop's response shifts from the sine form to an out-of-phase asymmetrical spreading. As noticed for all η, the drop attempts to regain its original height as the

voltage is reversed during the first half cycle, but the timescale is too short for the drop to regain the original height. In this middle height regaining process, the second increment in the voltage magnitude is triggered, i.e., the initiation of the second half of the cycle interrupts the recoiling and causes the drop to further spread. This causes the out-of-phase response, which intensifies along with the difference between the two valleys as Ro increases. As mentioned earlier, for higher Ro the drop spreading is minimal and is reversible in nature. The time to regain the original drop shape is strongly dependent on the viscosities of the drop and the medium. It would be interesting to see whether one can get similar reversibility in the air medium with the practical limitation of the contact angle hysteresis. One very critical aspect of the Young-Lippmann equation is scrutinized here: this classical equation never commented on the role of frequency. Here, we demonstrate that for Ro = 22.25 and above, the drop's response completely deviates from the expected prediction proposed by the Y-L equation. One can argue that only one cycle of actuation is applied, which motivated us to study the role of number of cycles, and the outcome was similar. The details of the role of number of cycles are presented in the upcoming sections, and prior to that, we have presented a quantified way to identify different regimes where the role of frequencies can be considered or ignored. In Fig. 2(c) an attempt is made to present a phase plot that can clearly identify the range in which one has to study the electrospreading.

Interestingly, if the minimum height attained by the drop is studied as a function of the Roshko number, the response resembling the S-shaped curve can be observed, as depicted in Fig. 2(c). This phase plot can be categorized into three different regimes, namely, regime I ($1 \gtrsim$ Ro), regime II ($20 \gtrsim$ Ro $\gtrsim 1$), and regime III (Ro $\gtrsim 20$). For regime I, where the applied frequency is smaller and can be approximated as dc electrowetting, the drop's response is approximately in phase with the applied actuation; hence, the minimum height is independent of Ro. Regime I is the process where the maximum drop deformation can be witnessed, which is in phase with the actuation, whereas regime II is out of phase of the drop's response. As identified in regime III, for very high actuation frequencies, the drop is irresponsive to the actuation; hence, it can be approximate as independent of the actuation. To further clarify the significance of the regimes, the theoretical response of the drop's height in three different regimes is presented in Fig. 2(d). In the first regime (regime I), when Ro $\ll 1$, the drop can closely follow the applied electrical field [18], but the minimum height deviates from the height calculated following the Y-L equation using the root-mean-square value of the voltage. However, it is desirable to reiterate that, for low frequencies, the drop response more closely resembles the dc voltage than the ac voltage, where the drop can spread to a greater extent. This justifies the deviation in the theoretical model from the experiments, in regime I, which underestimates the height reduction. In contrast, by increasing the actuation frequency at which electrowetting is triggered (higher Ro), the model perfectly predicts the response of the drop. For the transitional regime (regime II), when $20 \gtrsim$ Ro $\gtrsim 1$, the drop can partially follow the actuation, which leads to the out-of-phase behavior as explained in the case of variation of the η scenario. In this regime, the drop fails to attain the equilibrium maxima or minima in phase with the actuation. This has further consequences in terms of maximum spreading, which is a strong function of the number of actuation cycles that is studied in the upcoming section. For the last regime (regime III), when Ro > 20, the drop is completely irresponsive to the actuation cycle. In this particular case, the spreading becomes independent of η and Ro. The fact that a transitional regime exists can raise two questions: what would happen if more than a single sine wave is applied to the drop? And how many waves would be necessary to achieve the maximum reduction in height? Aiming to resolve the previous questions, the drop was subjected to a series of waves, and the minimum height achieved with respect to each cycle is studied and presented in Fig. 3(a). We believe the transition zone, i.e., regime II, is in between Ro = 2 and 22. Due to additional continuous actuation for a certain period, by means of a higher number of actuation cycles, the drop further spreads and attains the maximum possible spreading. This maximum spreading, after a certain number of actuation cycles, does not alter the maximum spreading or change the the contact angle. It is worthwhile to notice that the number of actuation cycles is strongly dependent on Ro: as Ro increases, one has to apply a larger number of cycles. Another interesting aspect was noticed regarding the drop's response
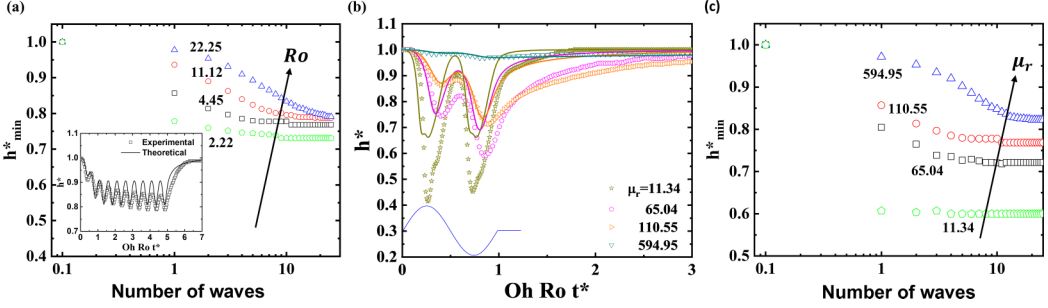
FIG. 3. (a) Minimum height achieved by a drop (Oh $= 0.009$ and $\mu_r = 110.55$) by a sequence of sine waves ($\eta = 0.65$) for different Roshko numbers. The initial height, when the number of waves is zero, is represented at 0.1 instead, because of the logarithmic nature of the plot. The maximum error obtained was $E_{h^*_{min}} = \pm 0.013$. The experimental results are represented by symbols and the results obtained from the proposed model are represented by solid lines. (b) Effect of viscosity ratio on drop spreading dynamics. Transient variation of the droplet height with additional terms fixed to Oh $= 0.009$, Ro $= 4.45$, and $\eta = 0.89$. (c) Minimum height achieved by a drop (Oh $= 0.009$ and Ro $= 4.45$) by a sequence of sine waves ($\eta = 0.65$) for different viscosity ratios. The maximum error obtained was $E_{h^*_{min}} = \pm 0.037$.

after this equilibration. As the inset of Fig. 3(a) shows, once this critical number of actuation cycles is performed, the drop deforms in phase with the actuation cycle. During the in-phase oscillatory behavior, the maximum and minimum drop height corresponds neither to the initial drop's height nor to the equivalent height predicted by the Y-L equation, respectively, due to the depletion of the lubricating layer sacrificing the reversibility of the system. In fact, as Ro is increased, more cycles are required to approach the in-phase cyclic response, as shown in Fig. 3(a). As a consequence of the higher number of cycles, the ultimate drop equilibrium height decreases with the increase in Ro. The higher Ro implies a faster spreading and a limited time for the drop to pursue the imposed actuation, which inevitably leads to a higher viscous dissipation and thus a longer time to achieve the equilibration. To the best of the authors' knowledge, based on all previous studies related to ac electrowetting, the researchers always comment that "sufficient time" was granted to the drop for this equilibration, but quantification of this sufficient time was missing, which we have presented here. For the completeness of the analysis, it is important to study the role of medium viscosity, as we present in the next section.

C. Effect of the viscosity ratio

For this paper, only the liquid medium viscosity was varied, and the viscosity ratio μ_r (ratio of the medium to the drop's viscosity) was always greater than 1, which implies that the effect of the work due to the medium dissipation was significantly higher than the drop viscous dissipation. However, both the drop and medium viscosity directly influence the relaxation time of the drop, by causing additional energy losses associated with energy dissipation. The study of viscosity ratios below unity can be easily performed in an air medium, but the existence of additional factors, such as evaporation and contact line friction, was restricting us to perform that spectrum. However, the proposed theoretical model can be used for the air medium. Figure 3(b) exhibits the experimental and theoretical response of a drop to a single wave for different viscosity ratios. A similar effect occurs for increasing the viscosity ratio, as in the case of increasing η and Ro, i.e., the drop cannot pursue the external actuation cycle. It requires more time to respond as the viscosity of the medium increases. The aforementioned delay is greatly reflected on the drop at the end of the first half of the cycle, where the drop cannot retract to its original height, and during the second half, the drop spreads in a completely different magnitude than the previous half. Thus, an irregular spreading is observed and more than one wave is required to attain the global minimum height. The

irregular response can be avoided by reducing the medium dissipation, accomplished by reducing the viscosity ratio, which guarantees insignificant losses due to the medium. For the least viscous medium in Fig. 3(b) ($\mu_r = 11.34$), the drop can retract to its original height by the end of the first half of the cycle, and the first and second valley are equal in magnitude. As μ_r increases, the drop's reaction diverges from the in-phase response and begins to lag. It can be observed in Fig. 3(b) that the lagging phenomenon and the intensified out-of-phase response can be seen with the increase in the viscosity ratio. For a more viscous medium, the difference between the first and second valley is more palpable and the reduction in the maximum height depression can be also witnessed. A clear similitude between Figs. 2(b) and 3(b) corroborates the statement that the transition of the drop's response from in phase to out of phase is linked to the relationship between the drop's response and the actuation timescale.

As we studied the role of number of cycles with the variations in Ro, a similar analysis is presented with respect to medium viscosity in Fig. 3(c). Also, it is observed that a plateau is reached after the actuation of a certain number of cycles beyond, in which the drop's response was in phase with the actuation independent of the number of waves. For higher viscosity ratios, the drop reduces the maximum spreading and requires more waves to reach the oscillatory steady state response. Thus, the resemblance between the Ro and the viscosity ratio is evident. Here again, the same observation was made that suggests a minimum number of cycles must be considered before commenting on the equilibration or even for the comparisons with the Y-L equation.

IV. CONCLUSION

This paper has developed a theoretical model to qualitatively predict the transient wetting dynamics of an electrolyte drop in viscous media to the actuation of an electric field. An overall energy balance approach was chosen to study the combined effects of the external driving, the surface tension, and the dissipation forces on the drop's oscillations. The model balances the energy delivered by the electrical actuation, which was simplified by defining an instantaneous contact angle as a function of a modified Young-Lippmann equation. The effect of three key parameters, i.e., η, Ro, and μ_r, is investigated to understand the importance of the magnitude of the actuation force, the dynamics involved in this force, and the viscosity of the system, respectively. This theoretical model, in corroboration with the experimental study, described the transient evolution of the drop motion from the initial position to the new equilibrium position and predicted the shift from in-phase to out-of-phase drop response from the applied waves. Moreover, three different regimes for the dynamic response of a sessile drop to electrowetting were identified. Finally, the effect of multiple waves on the dynamic response of an electrowetting drop is investigated. Therefore, we believe the proposed approach can provide a better understanding of the drop's dynamic wetting response under external actuations, like electric, magnetic, acoustic, and light.

ACKNOWLEDGMENTS

---

[1] F. Mugele and J.-C. Baret, Electrowetting: From basics to applications, J. Phys.: Condens. Matter **17**, R705 (2005).

[2] F. Mugele, J.-C. Baret, and D. Steinhauser, Microfluidic mixing through electrowetting-induced droplet oscillations, Appl. Phys. Lett. **88**, 204106 (2006).

[3] M. G. Pollack, R. B. Fair, and A. D. Shenderov, Electrowetting-based actuation of liquid droplets for microfluidic applications, Appl. Phys. Lett. **77**, 1725 (2000).

[4] F. Mugele, A. Staicu, R. Bakker, and D. van den Ende, Capillary stokes drift: A new driving mechanism for mixing in ac-electrowetting, Lab Chip **11**, 2011 (2011).

[5] B. Berge, Liquid lens technology: Principle of electrowetting based lenses and applications to imaging, in *Proceedings of the 18th IEEE International Conference on MEMS 2005* (IEEE, New York, 2005), pp. 227–230.

[6] X. Song, H. Zhang, D. Li, D. Jia, and T. Liu, Electrowetting lens with large aperture and focal length tunability, Sci. Rep. **10**, 16318 (2020).

[7] D. J. C. M. 't Mannetje, C. Murade, D. Van Den Ende, and F. Mugele, Electrically assisted drop sliding on inclined planes, Appl. Phys. Lett. **98**, 014102 (2011).

[8] X. Noblin, A. Buguin, and F. Brochard-Wyart, Vibrated sessile drops: Transition between pinned and mobile contact line oscillations, Eur. Phys. J. E **14**, 395 (2004).

[9] V. Srinivasan, V. K. Pamula, and R. B. Fair, An integrated digital microfluidic lab-on-a-chip for clinical diagnostics on human physiological fluids, Lab Chip **4**, 310 (2004).

[10] G. Lippmann, Relations entre les phénomènes électriques et capillaires, Ph.D. thesis, Gauthier-Villars, 1875.

[11] F. Li and F. Mugele, How to make sticky surfaces slippery: Contact angle hysteresis in electrowetting with alternating voltage, Appl. Phys. Lett. **92**, 244108 (2008).

[12] S. H. Ko, H. Lee, and K. H. Kang, Hydrodynamic flows in electrowetting, Langmuir **24**, 1094 (2008).

[13] Y. S. Nanayakkara, S. Perera, S. Bindiganavale, E. Wanigasekara, H. Moon, and D. W. Armstrong, The effect of ac frequency on the electrowetting behavior of ionic liquids, Anal. Chem. **82**, 3146 (2010).

[14] B. Majhy and A. Sen, Evaporation-induced transport of a pure aqueous droplet by an aqueous mixture droplet, Phys. Fluids **32**, 032003 (2020).

[15] T. B. Jones, J. D. Fowler, Y. S. Chang, and C.-J. Kim, Frequency-based relationship of electrowetting and dielectrophoretic liquid microactuation, Langmuir **19**, 7646 (2003).

[16] B. Majhy and A. Sen, Autonomous droplet transport on a chemically homogenous superhydrophilic surface, Colloids Surf. A **643**, 128798 (2022).

[17] T. B. Jones, K.-L. Wang, and D.-J. Yao, Frequency-dependent electromechanics of aqueous liquids: electrowetting and dielectrophoresis, Langmuir **20**, 2813 (2004).

[18] F. Hong, D. Jiang, and P. Cheng, Frequency-dependent resonance and asymmetric droplet oscillation under ac electrowetting on coplanar electrodes, J. Micromech. Microeng. **22**, 085024 (2012).

[19] J. M. Oh, S. H. Ko, and K. H. Kang, Shape oscillation of a drop in ac electrowetting, Langmuir **24**, 8379 (2008).

[20] J.-C. Baret, M. M. Decré, and F. Mugele, Self-excited drop oscillations in electrowetting, Langmuir **23**, 5173 (2007).

[21] S. Murali, K. P. Thompson, and J. P. Rolland, Three-dimensional adaptive microscopy using embedded liquid lens, Opt. Lett. **34**, 145 (2009).

[22] B. N. Ozbay, J. T. Losacco, R. Cormack, R. Weir, V. M. Bright, J. T. Gopinath, D. Restrepo, and E. A. Gibson, Miniaturized fiber-coupled confocal fluorescence microscope with an electrowetting variable focus lens using no moving parts, Opt. Lett. **40**, 2553 (2015).

[23] D. Erickson, B. Blackmore, and D. Li, An energy balance approach to modeling the hydrodynamically driven spreading of a liquid drop, Colloids Surf. A **182**, 109 (2001).

[24] J.-L. Lin, G.-B. Lee, Y.-H. Chang, and K.-Y. Lien, Model description of contact angles in electrowetting on dielectric layers, Langmuir **22**, 484 (2006).

[25] R. Zhao, L. Qi-Chao, W. Ping, and L. Zhong-Cheng, Contact angle hysteresis in electrowetting on dielectric, Chin. Phys. B **24**, 086801 (2015).

[26] See Supplemental Material at http://link.aps.org/supplemental/10.1103/PhysRevFluids.9.024001 for a detailed derivation of the mathematical model, electrical characterization of the EWOD system, and effect of voltage on contact angle; tables of properties of liquids used and nondimensional parameters for different combinations of physical variables; and movies of electrowetting induced reversible wetting

and dewetting of an aqueous droplet in the oil medium, and initial transient response of the aqueous droplet due to electrowetting. The Supplemental Material also contains Refs. [8,27–35].

[27] A. Ahmed, A. J. Qureshi, B. A. Fleck, and P. R. Waghmare, Effects of magnetic field on the spreading dynamics of an impinging ferrofluid droplet, J. Colloid Interface Sci. **532**, 309 (2018).

[28] J. C. Bird, S. Mandre, and H. A. Stone, Short-time dynamics of partial wetting, Phys. Rev. Lett. **100**, 234501 (2008).

[29] C. Hao, Y. Liu, X. Chen, Y. He, Q. Li, K. Li, and Z. Wang, Electrowetting on liquid-infused film (EWOLF): Complete reversibility and controlled droplet oscillation suppression for fast optical imaging, Sci. Rep. **4**, 6846 (2014).

[30] Y. Gu and D. Li, Liquid drop spreading on solid surfaces at low impact speeds, Colloids Surf. A **163**, 239 (2000).

[31] F. Brochard-Wyart and P. De Gennes, Dynamics of partial wetting, Adv. Colloid Interface Sci. **39**, 1 (1992).

[32] D. J. C. M. 't Mannetje, F. Mugele, and D. van den Ende, Stick–slip to sliding transition of dynamic contact lines under ac electrowetting, Langmuir **29**, 15116 (2013).

[33] M. Galiński, A. Lewandowski, and I. Stępniak, Ionic liquids as electrolytes, Electrochim. Acta **51**, 5567 (2006).

[34] A. A. Kornyshev, Double-layer in ionic liquids: paradigm change? J. Phys. Chem. B **111**, 5545 (2007).

[35] M. V. Fedorov and A. A. Kornyshev, Ionic liquids at electrified interfaces, Chem. Rev. **114**, 2978 (2014).

[36] A. Jha, P. Chantelot, C. Clanet, and D. Quéré, Viscous bouncing, Soft Matter **16**, 7270 (2020).

[37] M. Vallet, M. Vallade, and B. Berge, Limiting phenomena for the spreading of water on polymer films by electrowetting, Eur. Phys. J. B **11**, 583 (1999).

[38] H. Verheijen and M. Prins, Reversible electrowetting and trapping of charge: Model and experiments, Langmuir **15**, 6616 (1999).

[39] A. Roshko, On the development of turbulent wakes from vortex streets, NACA-TR-1191 (1954).

[40] C. Miller and L. Scriven, The oscillations of a fluid droplet immersed in another fluid, J. Fluid Mech. **32**, 417 (1968).